Fixed bed adsorption of CO$_2$/H$_2$ mixtures on activated carbon: experiments and modeling

Nathalie Casas · Johanna Schell · Ronny Pini · Marco Mazzotti

Abstract We present breakthrough experiments in a fixed bed adsorber packed with commercial activated carbon involving feed mixtures of carbon dioxide and hydrogen of different compositions. The experiments are carried out at four different temperatures (25 °C, 45 °C, 65 °C and 100 °C) and seven different pressures (1 bar, 5 bar, 10 bar, 15 bar, 20 bar, 25 bar and 35 bar). The interpretation of the experimental data is done by describing the adsorption process with a detailed one-dimensional model consisting of mass and heat balances and several constitutive equations, such as an adsorption isotherm and an equation of state. The dynamic model parameters, i.e. mass and heat transfer, are fitted to one single experiment (reference experiment) and the model is then further validated by predicting the remaining experiments. Furthermore, the choice of the isotherm model is discussed. The assessment of the model accuracy is carried out by comparing simulation results and experimental data, and by discussing key features and critical aspects of the model. This study is valuable per se and a necessary step toward the design, development and optimization of a pressure swing adsorption process for the separation of CO$_2$ and H$_2$ for example in the context of a pre-combustion CO$_2$ capture process, such as the integrated gasification combined cycle technology.

Keywords Pre-combustion CO$_2$ capture · PSA · Activated carbon · Breakthrough experiments · Simulations

N. Casas · J. Schell · M. Mazzotti (✉)
Institute of Process Engineering, ETH Zurich, Sonneggstrasse 3, 8092 Zurich, Switzerland
e-mail: marco.mazzotti@ipe.mavt.ethz.ch

R. Pini
Department of Energy Resources Engineering, Stanford University, Stanford, USA

Notation

a_p	specific surface of the adsorbent particles, [m^2/m^3]
a_w	cross section of the column wall, [m^2]
c	fluid phase concentration, [mol/m^3]
C_{ads}	heat capacity of the adsorbed phase, [J/(K kg)]
C_g	heat capacity of the gas, [J/(K m^3)]
C_g^{mol}	specific heat capacity of the gas, [J/(K mol)]
C_s	heat capacity of the solid, [J/(K kg)]
C_w	lumped heat capacity of the wall, [J/(K m^3)]
D_e	effective diffusion coefficient into the adsorbent particles [m^2/s]
D_L	axial dispersion coefficient [m^2/s]
D_m	molecular diffusion coefficient [m^2/s]
d_p	particle diameter, [m]
ΔH	heat of adsorption, [J/mol]
h_L	heat transfer coefficient (lumping column inside + wall), [J/(m^2 s K)]
h_W	heat transfer coefficient (lumping wall + heating), [J/(m^2 s K)]
k	overall mass transfer coefficient, [1/s]
K	Langmuir equilibrium constant, [1/Pa]
K_L	effective axial thermal conductivity in the fluid phase, [J/(m s K)]
L	column length [m]
N	number of species, [–]
N_{vol}	number of volume elements in the column, [–]
p	fluid pressure, [Pa]
q	solid phase concentration, [mol/kg]
q^*	solid phase concentration at equilibrium, [mol/kg]
q_s	solid phase concentration at saturation, [mol/kg]
R	ideal gas constant, [J/(K mol)]
R_i	inner column radius, [m]
R_o	outer column radius, [m]
s	exponent in Sips isotherm [–]

s_1 parameter for temperature dependent description of s, [–]

s_2 parameter for temperature dependent description of s, [–]

t time, [s]

T temperature, [K]

T_w wall temperature, [K]

T_{amb} ambient temperature, [K]

u superficial gas velocity, [m/s]

y mole fraction, [–]

z space coordinate in axial direction, [m]

Greek letters

ε_b bed void fraction, [–]

ε_t overall void fraction, [–]

θ parameter for temperature dependent description of q_s, [J/mol]

Θ parameter for temperature dependent description of K, [J/mol]

μ dynamic viscosity, [Pas]

ρ fluid phase density, [kg/m^3]

ρ_b bulk density of the packing, [kg/m^3]

ρ_p particle density, [kg/m^3]

ω parameter for temperature dependent description of q_s, [mol/kg]

Ω parameter for temperature dependent description of K, [1/Pa]

Sub- and Superscripts

feed   feed

i component i

init   initial

j component j

pipe   piping

Acronyms

BPR   back pressure regulator

CCS   Carbon Capture and Storage

EOS   Equation of State

IGCC   Integrated Gasification Combined Cycle

MSB   magnetic suspension balance

MFC   mass flow controller

MS   mass spectrometer

PDE   Partial Differential Equations

PSA   Pressure Swing Adsorption

TSA   Temperature Swing Adsorption

1 Introduction

The current emissions of carbon dioxide that originate mainly from the combustion of fossil fuels are approximately 30 GtCO$_2$/yr (U.S. Energy Information Administration 2011). At the same time, the concentration of CO$_2$ in the atmosphere is rapidly rising and approaches levels that may seriously and irreversibly endanger the climate (IPCC 2007). A complete transition to low-carbon and renewable energy sources—though indispensable—is not feasible within the near future. Bearing in mind the increasing energy requirements worldwide, Carbon Capture and Storage (CCS) is regarded as a possible bridging technology (IPCC 2005), allowing for a significant reduction of CO$_2$ emissions, while fossil fuels are still used.

Although CO$_2$ is routinely separated and produced as a by-product from industrial processes such as ammonia synthesis or hydrogen production, existing capture technologies are not cost-effective when considered in the context of sequestering CO$_2$ from power plants (U.S. Department of Energy 2010). New concepts of power plants are therefore investigated with increased efficiency and reduced CO$_2$ emissions. The Integrated Gasification Combined Cycle (IGCC) technology with pre-combustion CO$_2$ capture represents one of such options. Here, a fossil energy carrier such as coal is gasified using oxygen and steam, thus yielding carbon monoxide and hydrogen; these are further processed through the water-gas-shift reaction, whereby carbon monoxide is converted with H$_2$O to CO$_2$, hence producing additional hydrogen. The produced gas mixture leaves the reformer at high pressures (around 35 bar) and contains CO$_2$ at a fraction of about 40 %, the rest being mainly hydrogen. With respect to the subsequent separation process, this gas is therefore very different from the flue gas produced by a conventional power plant, where both the pressure and the CO$_2$ content are lower (atmospheric pressure and 3 to 15 vol.% CO$_2$ depending on the fuel used). As a consequence, an adsorption based separation process, especially Pressure Swing Adsorption (PSA), has promising characteristics for pre-combustion CO$_2$ capture.

In the PSA process, fixed bed adsorption columns are cyclically exposed to a high pressure feed step and to a low pressure regeneration step, in order to carry out the required separation, thus exploiting the pressure dependency of adsorption (Ruthven 1984). Various PSA processes were developed to date (Ruthven et al. 1994), most of them being designed to produce a weakly adsorbable species at a very high purity (>99.99 %). However, for a CO$_2$ capture process typical specifications are a high purity (>95 %) and capture rate (>90 %) of CO$_2$, i.e. the strongly adsorbed component on most adsorbents. This implies that a conventional PSA process (i.e. the so called Skarstrom cycle) is not applicable and that a different process concept has to be developed.

Additionally, the choice of the adsorbent material plays a crucial role in the process design; various tailor-made materials are currently being developed (Arstad et al. 2008; Belmabkhout and Sayari 2010; Herm et al. 2011) and have to be tested against commercially available adsorbents. To

this aim, the knowledge of both the thermodynamics and the kinetics of a given adsorbate/adsorbent system is required and can be studied by carrying out equilibrium adsorption isotherms measurements and breakthrough experiments, respectively.

PSA is not a novel technique, which depends on several coupled mechanisms (e.g. adsorption, mass and heat transfer). Therefore, the literature is vast and covers all different aspects of the behavior of fixed beds and of complete PSA processes; reviews of the literature can be found (Ruthven et al. 1994). In spite of such a body of literature there is a relatively little amount of studies and data about processes at high pressure and high temperature. This is in fact our area of interest with particular reference to the H_2/CO_2 separation on commercial activated carbon in the context of the pre-combustion CO_2 capture described above. The experimental conditions of most fixed bed studies are limited to low pressures (<2.5 bar) and moderate temperatures. The experimental full PSA investigations reported in the literature are in general carried out at pressures up to 10 bar (see for instance Malek and Farooq 1998; Zhou et al. 2005; Lopes et al. 2011; Mulgundmath et al. 2012), whereas few studies have considered pressures up to 20 bar (e.g. Kim et al. 1998, 2000; Taczyk and Warmuziski 1998). Another aspect which is only scarcely discussed in the literature, is the bulk gas separation, which is in fact important for pre-combustion CO_2 capture, as CO_2 concentrations up to 40 % have to be considered.

In this work we investigate the behavior of a non-isothermal fixed bed packed with activated carbon upon feeding of different CO_2/H_2 mixtures at temperatures between 25 °C and 100 °C and pressures between 1 bar and 35 bar. The experimental data are compared with simulation results obtained using a detailed model including adsorption isotherms measured earlier (Schell et al. 2012), and accounting for temperature effects. Such a model will be used for PSA process design in a follow up work.

2 Experimental

2.1 Materials and adsorption isotherms

A commercial activated carbon (AP3-60 from Chemviron Carbon, Germany) with a particle size of 3 mm was first thoroughly characterized by static adsorption measurements using a magnetic suspension balance (MSB) (Rubotherm, Bochum, Germany). The adsorption equilibria of interest for this work are reported and discussed in detail in an earlier paper (Schell et al. 2012). In particular, excess adsorption isotherms of pure CO_2 and H_2 have been measured in a wide pressure range (0.1 to 150 bar) at five different temperatures (25 °C, 45 °C, 65 °C, 100 °C and 140 °C), thus allowing to properly account for the temperature dependency

in the adsorption equilibrium isotherms determined through these data. This is an essential requirement for an accurate description of breakthrough experiments. The density of the activated carbon has been measured to be 1.97 g/cm^3 using a Helium pycnometer (AccuPyc 1330, Micromeritics, Brussels, Belgium).

All gases used in this work are obtained from Pangas (Dagmersellen, Switzerland) with purities >99.9 % for the pure gases; the CO_2/H_2 mixtures (25/75, 50/50 and 75/25) are produced by Pangas with relative errors of ±0.5 % to 3.0 %.

2.2 Experimental set up

All experiments are conducted in the one column adsorption set up shown in Fig. 1, where all basic steps of a PSA process, i.e. pressurization, adsorption, blowdown and purge, can be performed. However, this study addresses the adsorption step, hence only breakthrough experiments are carried out. The stainless steel column has a length of 1.2 m and an inner diameter of 2.5 cm. It is equipped with an electrical heater that is controlled using a thermocouple (Moser TMT AG, Hombrechtikon, Switzerland) mounted on the outer wall of the column. To assure an uniform heat distribution at the outer column wall the heating wire is embedded in two metal shells, whereby the inner shell is made out of cooper and the outer shell out of brass. The whole column is insulated (Insultech AG, Trimbach, Switzerland), to allow for experiments at different temperatures and to minimize heat losses at high temperature. Five additional thermocouples are positioned inside the column, i.e. at 10 cm, 35 cm, 60 cm, 85 cm and 110 cm with respect to the column inlet; the temperature of the gas entering and leaving the column is also monitored.

A mass flow controller (MFC) (Bronkhorst High-Tech BV, Ruurlo, The Netherlands) is used to control the feed flow rate. Its accuracy is reported to be higher than 2.5 %. However, the deviation can be larger in the vicinity of the minimum operating flow rate of the MFC.

The system pressure is maintained by a back pressure regulator (BPR) (Tescom, Elk River, USA) mounted downstream of the column. Additionally, the pressure drop across the bed is measured using two pressure transducers (Keller, Jestetten, Germany) installed at the inlet and at the outlet of the column. A combination of automatically and manually activated valves allows for a flexible choice of the feeding route; the operation is controlled through the LabVIEW software, enhanced by the use of virtual instruments (VIs) that have been developed specifically for this setup. On-line monitoring of the outlet gas composition is done using a mass spectrometer (MS) (Pfeiffer Vacuum Schweiz AG, Switzerland).
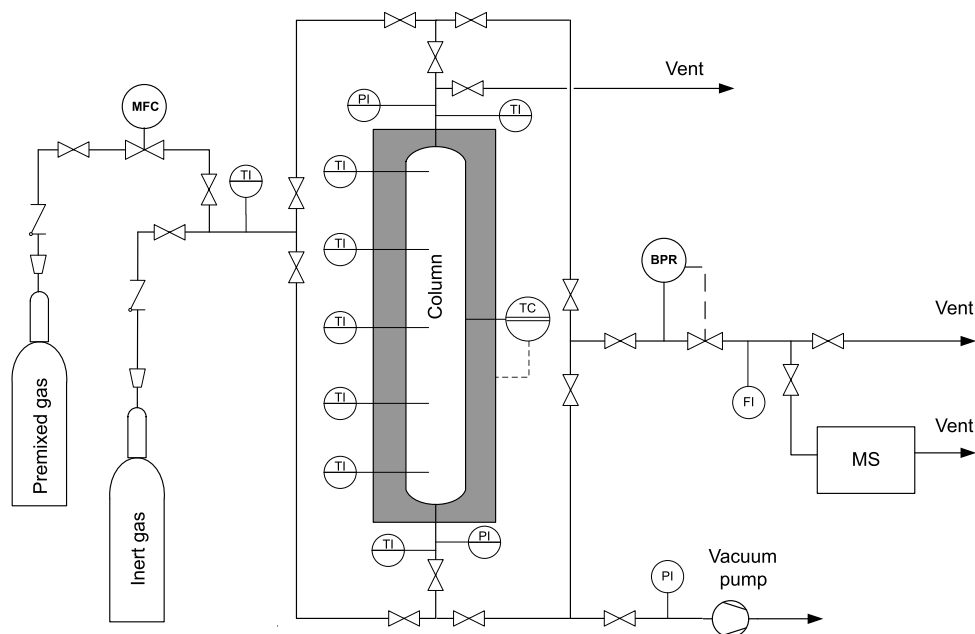
2.3 Experimental procedure

Prior to each experiment, the MS is calibrated using the
certified premixed CO_2/H_2 mixtures. The column is first
heated to the experimental temperature and then brought to
the desired pressure using Helium (inert); once the targeted
pressure is reached, the feed is switched to the CO_2/H_2 mix-
ture of choice and its flow rate is maintained by the MFC at a
value of 10 cm^3/s. Note that although all experiments have
been performed at the same feed velocity, the molar flow
rate changes depending on gas composition, pressure and
temperature.

The adsorbent is regenerated before each experiment by
applying vacuum for 45 minutes. After a series of max-
imum four experiments the column is regenerated under
more drastic conditions, i.e. by maintaining it at 150 °C un-
der vacuum for 1 h 30 min. The latter regeneration proce-
dure is not conducted before each experiment in the interest
of time; a comparison between two experiments carried out
after either type of regeneration does not exhibit any signif-
icant difference.

In this study, experiments are carried out at four different
temperatures (25 °C, 45 °C, 65 °C and 100 °C) and seven
different pressures (1 bar, 5 bar, 10 bar, 15 bar, 20 bar, 25 bar
and 35 bar) feeding three different CO_2/H_2 mixtures, with
CO_2/H_2 concentrations of 25/75, 50/50 and 75/25. More-
over, experiments at four different feed flow rates are con-
ducted (10, 20, 30 and 40 cm^3/s).

3 Modeling

In this section the mathematical model used to describe
the breakthrough experiments is presented. It is important
to provide the details of the modeling approach, which is
adapted to the high pressure and temperature conditions of
the experiments and of the PSA process, for the design of
which the model is developed.

3.1 Material and energy balances

A one-dimensional column model including mass and en-
ergy balances is used to describe the column experiments.
The mass transfer between the fluid and the solid phase as
well as heat transfer from inside the column to the envi-
ronment are described using lumped equations. For the heat
transfer the geometry of the column wall plays a crucial role.
Therefore, also the heating system including its metal shells
described in Sect. 2.2 have to be considered for the correct
description of heat transfer. The following assumptions are
made:

- Negligible radial temperature and concentration gradi-
  ents.
- Thermal equilibrium between the fluid and the adsorbent
  particles.
- No axial conductivity along the column wall.
- The column wall properties are calculated by lumping the
  properties of the different metal layers.
- The temperature of the environment that surrounds the
  column and with which heat transfer takes place, T_{amb},
  is fixed to be equal to the set point of the heating.
- Temperature independent mass transfer coefficients, isos-
  teric heats of adsorption and heat capacities of the solid
  phase and the wall.
- Mass transfer resistance described using a linear driving
  force (LDF) model.

– The piping from the column to the mass spectrometer, where the breakthrough profiles are measured, is described with an isothermal plugflow model.

Considering all the assumptions, the overall and component mass balances are given as follows:

$$\varepsilon_t \frac{\partial c}{\partial t} + \frac{\partial (uc)}{\partial z} + \rho_b \sum_{j=1}^{n} \frac{\partial q_j}{\partial t} = 0 \tag{1}$$

$$i = 1, \ldots, N$$

$$\varepsilon_t \frac{\partial c_i}{\partial t} + \frac{\partial (uc_i)}{\partial z} + \rho_b \frac{\partial q_i}{\partial t} - \varepsilon_b \frac{\partial}{\partial z}\left(D_L c \frac{\partial y_i}{\partial z} \right) = 0 \tag{2}$$

where c is the total fluid phase concentration, c_i and q_i are the fluid and the adsorbed phase concentration of species i; u, ε_t and ε_b are the superficial gas velocity, the overall and the bed void fraction, respectively; ρ_b represents the bulk density of the packing in the column, i.e. the mass of the adsorbent loaded in the column divided by the bed volume; D_L is the axial dispersion coefficient, which is assumed to be the same for all species; t and z are the time and space coordinates.

The diffusion in the solid is considered to be rate limiting, hence the mass transfer rate is expressed using the following linear driving force (LDF) model (lumped solid diffusion model):

$$\frac{\partial q_i}{\partial t} = k_i \left(q_i^* - q_i \right) \quad i = 1, \ldots, N \tag{3}$$

where $k_i = k_{f,i} a_p$ and $k_{f,i}$ is the component specific lumped mass transfer coefficient and a_p the specific surface area of the adsorbent particles; q_i^* is the adsorbed phase concentration in equilibrium with the bulk of the gas phase, which is calculated using the competitive adsorption isotherm depending on temperature and partial pressures:

$$q_i^* = f_i^{eq}(T, p_1, p_2, \ldots, p_N) \quad i = 1, \ldots, N \tag{4}$$

To account for heat effects and temperature changes during the adsorption process and along the column, two energy balances are needed. The energy balance for the fluid and solid phases inside the column, including the term accounting for heat transfer to the column wall, can be written as follows:

$$(\varepsilon_t C_g + \rho_b C_s + \rho_b C_{ads}) \frac{\partial T}{\partial t} - \varepsilon_t \frac{\partial p}{\partial t}$$
$$+ u C_g \frac{\partial T}{\partial z} - \rho_b \sum_{j=1}^{n} (-\Delta H_j) \frac{\partial q_j}{\partial t}$$
$$+ \frac{2h_L}{R_i}(T - T_w) - \varepsilon_b \frac{\partial}{\partial z}\left(K_L \frac{\partial T}{\partial z} \right) = 0 \tag{5}$$

where T and T_w are the temperature in the column and at the column wall, respectively; C_g, C_s and C_{ads} are the heat capacities of the fluid, the solid and the adsorbed phase, respectively; ΔH_j is the isosteric heat of adsorption of species j; h_L is the heat transfer coefficient from inside the column to the column wall; R_i is the column inner radius and K_L is the axial thermal conductivity. An energy balance around the column wall accounts for the heat transfer from the wall to the outside:

$$\frac{\partial T_w}{\partial t} = \frac{2\pi}{C_w a_w}\big(h_L R_i (T - T_w) - h_w R_o (T_w - T_{amb}) \big) \tag{6}$$

where h_w and C_w are the heat transfer coefficient from the wall to the environment and the lumped heat capacity of the column wall and the heating system, respectively; a_w is the cross section of the column wall and R_o the outer column radius including the heating system.

The boundary conditions of the system can be written as follows:

for the inlet: $z = 0$

$$u_{feed} c_{feed} = uc$$

$$u_{feed} c_{i,feed} = uc_i - \varepsilon_b D_L c \frac{\partial y_i}{\partial z}$$

$$u_{feed} C_{g,feed} T_{feed} = u_{feed} C_{g,feed} T - \varepsilon_b K_L \frac{\partial T}{\partial z}$$

for the outlet: $z = L$

$$\frac{\partial c_i}{\partial z} = 0$$

$$\frac{\partial T}{\partial z} = 0$$

$$p = p_{out}$$

and the initial conditions at $t = 0$ for $0 \leq z \leq L$ are given as:

$$c = c_{He}, \qquad c_{CO_2} = c_{H_2} = 0$$

$$T = T_{init}, \qquad T_w = T_{amb}$$

The Partial Differential Equations (PDEs) are discretized in space into N_{vol} finite volumes with a constant width Δz, where z_i denotes the cell center and $z_{i\pm 1/2}$ indicates the cell boundaries. As a consequence:

$$z_{1/2} = 0 \quad \text{and} \quad z_{N_{vol}+1/2} = L$$

The flux limiter used in this work is calculated applying the VanLeer method described in LeVeque (2002). The implementation of the finite volume method for adsorption column models is described in more detail in Webley and He (2000) and Javeed et al. (2011). Time integration is performed with the commercial IMSL DIVPAG solver (Fortran) according to Gear's method.

3.2 Modeling of the piping system

In contrast to the temperatures, which are measured inline, the gas composition is measured downstream of the column. Due to the volume of the lines connecting the column outlet to the MS, the concentration measurement is carried out with a certain delay with respect to when the gas leaves the column. Moreover, in this volume there is also some additional dispersion that might affect the measurement. Such effects have to be carefully accounted for in order to enable the comparison between experimental data and simulation results. Due to the changing compositions and flowrates in this part of the experimental set up, a simple time adjustment of the experimental profiles is not possible. Therefore, one must include in the model also the description of the flow through the tubing and valves between the column outlet and the MS detector. To describe this, the following total and component mass balances along the piping are written, by assuming constant temperature and volumetric behavior:

$$\frac{\partial c^{\text{pipe}}}{\partial t} + \frac{\partial (u^{\text{pipe}} c^{\text{pipe}})}{\partial z} = 0 \tag{7}$$

$$i = 1, \ldots, N$$

$$\frac{\partial c_i^{\text{pipe}}}{\partial t} + \frac{\partial (u^{\text{pipe}} c_i^{\text{pipe}})}{\partial z} - \frac{\partial}{\partial z}\left(D_{\text{L}}^{\text{pipe}} c^{\text{pipe}} \frac{\partial y_i^{\text{pipe}}}{\partial z}\right) = 0 \tag{8}$$

For the sake of simplicity, the piping system is modeled as a pipe of uniform cross section divided in two parts, characterized by a high and a low pressure regions, and assuming constant pressure and velocity in each of these two parts. The initial conditions are the same as in the adsorption column, and the boundary condition at the pipe inlet corresponds to the composition at the outlet of the adsorption column.

3.3 Constitutive equations

3.3.1 Equation of State (EOS)

In this study the ideal gas law is used to describe the fluid phase behavior:

$$c_i = \frac{y_i p}{RT} \tag{9}$$

This is reasonable considering that the compressibility factor calculated using the Peng-Robinson EOS is between 0.9 and 1 for all investigated CO_2/H_2 mixtures under all conditions (p, T) considered here.

3.3.2 Pressure drop

The gas velocity in the column is calculated by solving the Ergun equation for a given pressure gradient along the column:

$$\frac{\partial p}{\partial z} = -\frac{150\mu(1-\varepsilon_{\text{b}})^2}{\varepsilon_{\text{b}}^3 d_{\text{p}}^2} u - \frac{1.75(1-\varepsilon_{\text{b}})\rho}{\varepsilon_{\text{b}}^3 d_{\text{p}}} |u|u \tag{10}$$

where ρ and μ are the fluid density and the dynamic viscosity, respectively; d_p is the particle diameter.

3.3.3 Heat capacity of the gas and the adsorbed phase

Since the system is non-isothermal and the composition of the gas phase changes along the column over time, the heat capacity of the fluid, C_{g}, and the heat capacity of the adsorbed phase, C_{ads}, depend on the fluid concentration, c_i, and the adsorbed phase concentration, q_i, respectively:

$$C_{\text{g}} = \sum_i^N c_i C_{\text{g},i}^{\text{mol}} \quad i = 1, \ldots, N \tag{11}$$

$$C_{\text{ads}} = \sum_i^N q_i C_{\text{g},i}^{\text{mol}} \quad i = 1, \ldots, N \tag{12}$$

where the specific heat capacity of species i, $C_{\text{g},i}^{\text{mol}}$, is chosen to be an average over a temperature range from 298 K to 373 K at 15 bar. Following this approach, C_{g} is still underestimated for pressures higher than 15 bar, but the advantage is that the obtained expression is simple and can be easily implemented in the model.

3.3.4 Adsorption isotherms and isosteric heat of adsorption

Two different single component adsorption isotherms are considered, namely the Langmuir and the Sips isotherm (Do 1998), which can be written in the following general form:

$$q_i^* = \frac{q_{\text{si}}(K_i p)^{s_i}}{1 + (K_i p)^{s_i}} \tag{13}$$

where q_i^* is the adsorbed phase concentration in equilibrium with the gas phase, p is the pressure and q_{si} and K_i are the saturation capacity and the adsorption equilibrium constant of component i. The third parameter s_i accounts for the inhomogeneity of the adsorption surface; if the adsorbent surface is assumed to be homogeneous, as it is the case for the Langmuir isotherm, s_i is 1.

The CO_2 isotherms, which were reported earlier in Schell et al. (2012), are shown in Fig. 2, which is limited to the pressure range of interest here. Although both isotherm models provide a good description of the experimental data, the Sips isotherm follows the low pressure data points better than the Langmuir isotherm.
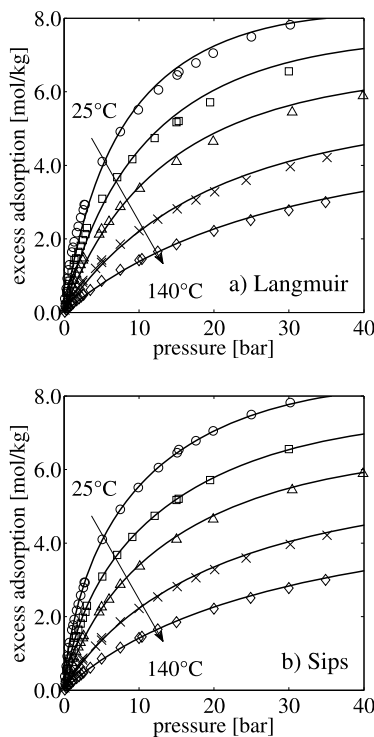
Fig. 2 Excess adsorption of pure CO_2 on activated carbon in the pressure range of interest ($p \leq 40$ bar). Experimental data are the same in both figures and correspond to those reported earlier; they are given in terms of excess adsorption as explained in the original paper (Schell et al. 2012). Two different isotherm models are plotted: (**a**) Langmuir isotherm and (**b**) Sips isotherm, where the symbols are the experimental values and the lines represent the fit using the corresponding isotherm model at different temperatures: 25 °C *circles*, 45 °C *squares*, 65 °C *triangles*, 100 °C *crosses*, 140 °C *diamonds*. The isotherm equation (13), which gives absolute adsorbed amounts, is converted to excess adsorption by using equation (4) in Schell et al. (2012). Note that to be consistent with the original experimental data, the units on the vertical axis have been changed to *per unit mass* using the particle density ρ_p

The temperature dependency of the three isotherm parameters is accounted for by the following equations:

$$i = 1, \ldots, N$$

$$q_{si} = \omega_i \exp\left(\frac{-\theta_i}{RT}\right) \tag{14a}$$

$$K_i = \Omega_i \exp\left(\frac{-\Theta_i}{RT}\right) \tag{14b}$$

$$s_i = s_{1i} \operatorname{atan}\left(s_{2i}(T - T_{\text{ref},i})\right) + s_{\text{ref},i} \tag{14c}$$

The corresponding parameter values are reported in Table 4. Finally, an empirical competitive adsorption isotherm is constructed from the pure component isotherms as follows:

$$q_i^* = \frac{q_{si}(K_i p_i)^{s_i}}{1 + \sum_{j=1}^{n}(K_j p_j)^{s_j}} \quad i = 1, \ldots, N \tag{15}$$
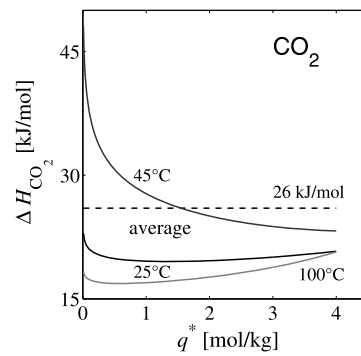

Fig. 3 Isosteric heat of adsorption for pure CO_2 on activated carbon at 25 °C, 45 °C and 100 °C as obtained using the Clausius Clapeyron equation (Schell et al. 2012). Note that the corresponding curves at 65 °C and 140 °C are very close to those at 45 °C and 100 °C, respectively (Schell et al. 2012). The average isosteric heat of adsorption (*dashed line*) is the value used in the simulation, namely 26 kJ/mol

We have shown earlier that ΔH_i depends on the amount adsorbed as well as on temperature (Schell et al. 2012). The data for CO_2 at three different temperatures in the range of interest is shown in Fig. 3. In the model an average ΔH_i for each component is used as given for CO_2 by the dashed line in Fig. 3. This leads to an underestimation of ΔH_i at low loadings particulary in the temperature range of 45 °C and 65 °C, and an overestimation at CO_2 loadings larger than 2 mol/kg.

3.4 Predictive correlations for model parameters

The model parameters, which are defined a priori, such as the physical properties of the adsorption material, the thermodynamical fluid properties and the adsorption properties which can be extracted from the equilibrium adsorption isotherms, are summarized in Table 2. This leaves us with four parameters that have to be fitted to the experimental data, namely the heat transfer coefficient between column inside and wall h_L, the heat transfer coefficient between wall and the outside h_W and the mass transfer coefficients for CO_2 and H_2. For the fitting it is important to have reasonable initial values, therefore estimates are calculated using correlations. All estimates are calculated for reference conditions: 15 bar, 25 °C and a 50/50 CO_2/H_2 mixture.

As discussed above the mass transfer is described with a lumped mass transfer coefficient k_i. A first guess for k_i is obtained from the Glueckauf's expression (Kim et al. 1994), which is given by:

$$k_i = \frac{60 D_e}{d_p^2} \tag{16}$$

where d_p is the particle diameter and D_e is the effective diffusivity coefficient into the adsorbent particles, which is found to be strongly system dependent. Data between

Table 1 Overview of the experiments conducted at four different temperatures (25 °C, 45 °C, 65 °C and 100 °C) and seven different pressures (1 bar, 5 bar, 10 bar, 15 bar, 20 bar, 25 bar and 35 bar) feed-ing three different CO_2/H_2 mixtures, with CO_2/H_2 concentrations of 75/25, 50/50 and 25/75

CO_2/H_2	25/75							50/50						75/25					
P [bar]	1	5	10	15	20	25	35	5	10	15	20	25	35	5	10	15	20	25	35
T [°C]																			
25	x	x	x	x	x	x	x	x	x	x	x	x	x	x	x	x	x	x	x
45	–	x	x	x	–	x	–	x	x	x	–	x	–	x	x	x	–	x	–
65	–	–	–	x	–	–	–	–	–	x	–	–	–	–	–	x	–	–	–
100	–	–	–	x	–	–	–	–	–	x	–	–	–	–	–	x	–	–	–

Table 2 Model parameters

Parameter		Origin	Value
Column length	L	Equipment	1.20 [m]
Inner column radius	R_i	Equipment	0.0125 [m]
Outer column radius (lumped)	R_0	Equipment	0.02 [m]
Bed porosity	ε_b	Measured	0.403 [–]
Total porosity	ε_t	Calculated	0.742 [–]
Bulk density of the packing	ρ_b	Measured	507 [kg/m^3]
Particle density	ρ_p	Manufacturer[a]	850 [kg/m^3]
Particle size	d_p	Manufacturer	0.003 [m]
Specific surface area	a_p	Manufacturer	8.5×10^8 [m^2/m^3]
Solid heat capacity	C_s	Manufacturer	1000 [J/K kg]
Heat capacity of the wall (lumped)	C_w	Manufacturer	4×10^6 [J/K m^3]
Fluid heat capacity	$C_{g,i}^{mol}$	Calculated[b]	[J/K m^3]
Molecular Diffusion	D_m	Calculated[c]	4.3×10^{-6} [m^2/s]
Diffusion in the piping	D_L^{pipe}	Fixed	0 [m^2/s]
Isotherm parameters		Static measurements	Table 4
Heat of adsorption CO_2	ΔH_{CO_2}	Clausius-Clapeyron	−26000 [J/mol]
Heat of adsorption H_2	ΔH_{H_2}	Clausius-Clapeyron	−9800 [J/mol]
Mass transfer coefficient	k_i	Dynamic measurements	Table 3 [1/s]

[a]Chemviron carbon

[b]Average over a temperature range 298 K–373 K at 15 bar (NIST 2011)

[c]Calculated for a 50/50 CO_2/H_2 mixture at 298 K and 15 bar using a reference value (Haynes 2011)

1×10^{-7} m^2/s and 1×10^{-8} m^2/s are reported (Ruthven 1984), hence a value of $D_e = 5 \times 10^{-8}$ m^2/s was chosen as a starting point.

A first estimation of the heat transfer coefficient h_L was obtained by Leva's correlation (Leva 1947):

$$Nu \equiv \frac{h_L 2R_i}{K_L} = 0.813 Re^{0.9} \exp(-6d_p/2R_i) \qquad (17)$$

where R_i, d_p and K_L are the column inner radius, the particle diameter and the axial thermal conductivity, respectively; Re represents the Reynolds number which is dependent on the velocity, fluid density and viscosity. The heat transfer at the outer wall surface h_W is described by natural convection

and can be estimated by the following correlation (Perry et al. 1984):

$$h_W = b_n(\Delta T)^m (2R_o)^{3m-1} = 3.32(\Delta T)^{0.25} \qquad (18)$$

The values of b_n and m are given in Perry et al. (1984) and depend on the dimensionless numbers Prandtl and Grashof, which are in turn dependent on fluid properties such as density, viscosity and heat capacity; ΔT is set to be 50 °C, corresponding to the temperature increase due to adsorption during the reference experiment (15 bar, 25 °C and a 50/50 CO_2/H_2 feed).

Since the mass transfer coefficient is fitted to the break-through curves, axial dispersion must be accounted for in the

simulations in order to differentiate this effect from mass transfer resistance. The dispersion coefficient D_L is calculated accounting for the molecular diffusion and the turbulent mixing (Ruthven 1984):

$$D_L = \gamma_1 D_m + \gamma_2 d_p u/\varepsilon \qquad (19)$$

where D_m is the molecular diffusion and u/ε the interstitial velocity. The factors γ_1 and γ_2 account for the tortuosity and turbulent mixing, respectively, and typical values of 0.7 and 0.5 (Ruthven 1984) are used. The thermal conductivity coefficient K_L is given by $K_L = D_L C_g$ as the convective heat and mass transport are dominated by the same mechanism (Ruthven 1984).

4 Results

In the following experimental and simulated breakthrough data in a wide range of process conditions are evaluated and different model assumptions are discussed. To enable this comparison, the dynamic model parameters, i.e. mass and heat transfer, are fitted to one single experiment (reference experiment) and the validated model is then used to predict the remaining experiments.

An overview of all experiments conducted in this study is shown in Table 1. Several of the presented experiments have been repeated and show an excellent reproducibility. Moreover, the effect of the feed flow rate on the mass transfer and consequently on the breakthrough profiles, is found to be negligible in the area of interest.

The heating system proved to be inadequate for operation above 60 °C. Therefore, the experiments at high temperature cannot be compared to the others, hence will not be further discussed.

4.1 Reference breakthrough experiment

As an example of the general behavior, the reference experiment (15 bar, 25 °C and a 50/50 CO_2/H_2 feed), shown in Fig. 4, is discussed. It shows the concentration profiles of CO_2 and H_2 measured by the MS, as well as the temperature profiles monitored within the column. Symbols represent the experimental values, whereas lines give results from simulations, which are discussed in more detail in Sect. 4.2 and Sect. 4.3. The observed concentration profiles are characterized by three distinct regions: (1) in the initial state Helium is displaced and produced (not shown in Fig. 4 as $y_{He} = 1 - y_{CO_2} - y_{H_2}$), (2) hydrogen breakthrough and production of pure hydrogen, (3) CO_2 breakthrough and transient to reach the composition of the feed. Besides the feed velocity, the breakthrough time depends on the adsorption capacity at given conditions (composition, pressure and temperature), thus providing a good indication of the separation potential of the investigated adsorbate-adsorbent system.
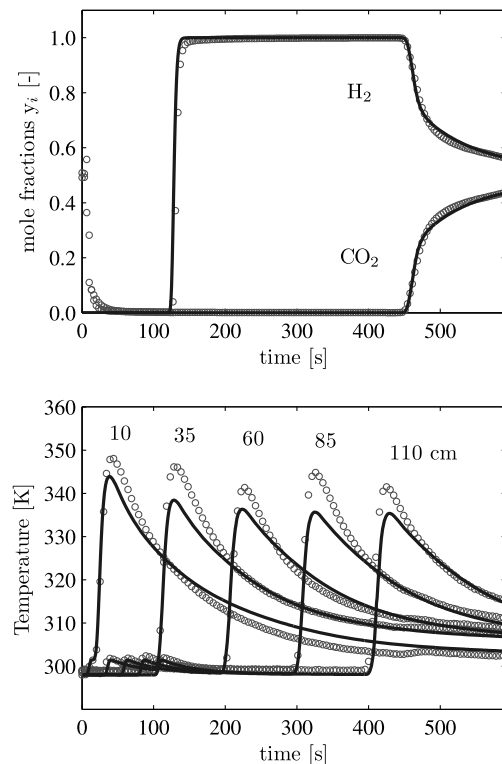

Fig. 4 Reference experiment (50/50 feed, 15 bar and 25 °C) to which the parameter are fitted to

Since adsorption is an exothermic process, the temperature in the column changes significantly during adsorption, thus allowing through the temperature profiles to indirectly track the position of both the H_2 and CO_2 fronts. The temperature profiles monitored at five different locations in the column (10 cm, 35 cm, 60 cm, 85 cm and 110 cm) are shown in Fig. 4 as a function of time. At each position two different temperature peaks are observed, corresponding to the H_2 front (small temperature increase) and to the CO_2 front (large temperature increase). Note that at 10 cm, the temperature peaks of H_2 and CO_2 coincide, as the two fronts are very close to each other and the corresponding temperature variations occur almost at the same time.

As discussed above, H_2 moves faster than CO_2 through the column: the temperature peak at 110 cm is measured at about 110 s, which corresponds to the H_2 breakthrough time observed in Fig. 4. Additionally, the characteristic shape of the temperature peaks results from a combination of both mass and heat transfer: the sharp initial front indicates fast mass transfer, whereas the shape of the tail is controlled by the heat transfer from the column to the environment. The latter is furthermore responsible for the time required to reach the feed composition at the outlet of the column, once CO_2 breakthrough is observed. As long as the column temperature is decreasing and has not reached its initial value, CO_2 is further adsorbed, as the adsorption capacity is higher

Table 3 Estimated and fitted mass and heat transfer coefficients, as well as the two parameter used in the description of the Nusselt number

	k_{CO_2} [s^{-1}]	k_{H_2} [s^{-1}]	h_W [J/(m^2 s K)]	η_1 [–]	η_2 [–]
From correlations	0.33	0.33	8.8	0.813	0.9
From experiments	0.15	1.0	5	41.13	0.32

Table 4 Parameters to describe the Langmuir and Sips isotherms temperature dependent (Schell et al. 2012); the temperature dependencies of q_{si} and K_i are both described with an Arrhenius type equation, whereas the temperature dependence of s_{CO_2} is described with an inverse tangent. No temperature dependence is observed for q_{si} and s_i in the case of H_2 adsorption

				CO$_2$	H$_2$
Langmuir					
q_{si}	[mol/m^3]	ω_i	[mol/kg]	2.07	5.35
		θ_i	[J/mol]	−4174	0
K_i	[1/Pa]	Ω_i	[1/Pa]	5.59×10^{-9}	0.88×10^{-9}
		Θ_i	[J/mol]	−13133	−10162
Sips					
q_{si}	[mol/m^3]	ω_i	[mol/kg]	1.38	6.66
		θ_i	[J/mol]	−5628	0
K_i	[1/Pa]	Ω_i	[1/Pa]	16.80×10^{-9}	0.70×10^{-9}
		Θ_i	[J/mol]	−9159	−9826
s_i	[–]	s_{1i}	[–]	0.072	0
		s_{2i}	[1/K]	0.106	0
		$s_{ref,i}$	[–]	0.827	0.9556
		$T_{ref,i}$	[K]	329	273

at lower temperatures. This readsorption leads to a flattening of the CO$_2$ front.

4.2 Parameter estimation

The description of the experimental data and the fitting of the missing model parameter is done using the mathematical model defined in Sect. 3, and the adsorption equilibrium is described using multi-component Sips isotherm.

The four parameters discussed in Sect. 3.4, namely the two heat transfer parameters as well as the mass transfer parameters are fitted to the reference experiment (15 bar, 25 °C and a 50/50 CO$_2$/H$_2$ feed), which is shown in Fig. 4, where the symbols and the solid lines represent the experimental and the simulated data, respectively. The two mass transfer parameters and the heat transfer parameter from the wall to the environment, h_W, are assumed to be a constant. In order to describe accurately the heat transfer coefficient from inside the column to the column wall, h_L, the Nusselt number defined in equation (17) is written in a more general form:

$$Nu \equiv \eta_1 Re^{\eta_2} \exp(-6d_p/2R_i)$$

where the two parameters η_1 and η_2 are then fitted to the experimental data. The experimental data can be described by the presented model using the fitted parameters reported in Table 3. The comparison between simulations and experiments is rather satisfactory. However, the simulated temperature profiles are somewhat lower than the experimental ones, see Fig. 4. This discrepancy could on the one hand be explained by the use of a constant isosteric heat of adsorption. On the other hand it could also be a consequence of neglecting the radial temperature profile in the column. With reference to Table 3, it is worth noting that there are large differences between the values of the model parameters estimated by fitting the experimental results and those estimated using the correlations reported in Sect. 3.4. These differences in the parameters' values correspond to large and unacceptable differences between predicted and measured concentration and temperature profiles, as shown in Fig. 5. They should not surprise however, since similar differences, particularly in the correlation for the Nusselt number, have been reported by others (Rohsenow et al. 1985; Ruthven 1984; Lin and Farooq 1999). Our conclusion is that these parameters have to be estimated from experiments carried out in the range of conditions (geometry, flows, etc.) of interest.

In order to challenge the choice of the Sips adsorption isotherm, we have tried to fit the low pressure experiments
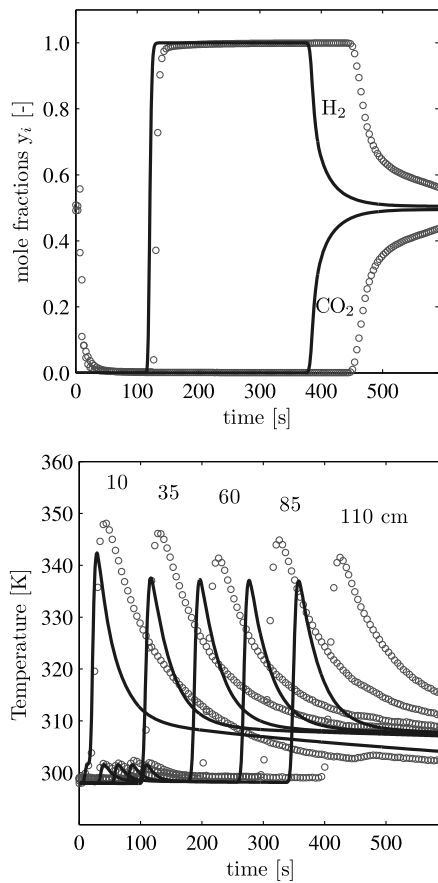
Fig. 5 Comparison of the simulated exit and temperature profiles using the first estimates to describe the mass and heat transport parameters with the reference experiment (50/50 feed, 15 bar and 25 °C)

($p = 5$ bar) using the Langmuir isotherm. However, it was not possible to find a set of mass and heat transfer parameters that would reproduce at least qualitatively the temperature profiles in the column. It is remarkable that the small, but clear, difference that we see in the quality of the fitting of the adsorption equilibrium data at low pressure when using the Sips isotherm instead of the Langmuir isotherm, yields such a significant difference in the description of the fixed bed experiments. Such observation confirms that the Sips isotherm is indeed the best model to describe the competitive adsorption of CO_2 and H_2 on this activated carbon.

4.3 Prediction of breakthrough experiments

The model that has been calibrated to one single experiment, is now used to predict the breakthrough and the temperature profiles of the remaining experiments. Figures 6 and 7 show the composition and temperature profiles for the experiments carried out at 25 °C, whereas the corresponding profiles measured at 45 °C are reported in Figs. 8 and 9. In general, a good agreement is obtained between experimental

(symbols) and simulated (lines) data over the whole range of temperature, pressure and compositions.

A comment has to be made with respect to the experiments carried out at 25 °C and 5 bar (Fig. 6), and at 45 °C and 10 bar (Fig. 8) where a 75/25 CO_2/H_2 mixture is fed. It is apparent that under these two conditions the experimental exit profiles are not as smooth as for all other experiments and that the agreement between experiments and simulations after CO_2 breakthrough is less satisfactory. The experimental practice has shown that the back pressure regulator (BPR) has some difficulties in controlling the pressure in the system, when the actual outlet flow rate is much lower compared to the one used during initial pressurization with Helium. This situation arises whenever one or more components have a high adsorption capacity and the feed flow rate is rather low; it is therefore pronounced at high CO_2 concentrations and low pressure. From a practical point of view instabilities in the pressure are reflected in the adsorption behavior inside the column and in turn in the composition of the fluid phase. Moreover, the effect on the latter is particularly strong at low pressures, where the adsorption isotherm is rather steep (see Fig. 2).

Furthermore, it has to be mentioned that the feed velocity used in the simulations had to be adjusted in order to match the temperature profiles in the column. Figure 10 shows the relative deviations between the feed velocity used in the simulation and the setpoint assigned in the experiment (relative error = $(u_{exp} - u_{sim})/u_{exp}$). A positive value of the relative error indicates a smaller velocity in the simulation as compared to the experimental setpoint and vice versa. Different effects could be responsible for this deviation, which is sometimes rather large.

On the one hand, there might be a mismatch between model and experimental system, e.g. in terms of heat of adsorption or of the thermostatting system. The model is indeed very sensitive to the details of the description of heat effects, particularly regarding temperature and adsorption capacity. These effects are strongly coupled to the set velocity, which changes along the bed because of gas adsorption and associated thermal effects. Even though the agreement between simulations and experiments is in general good, some deviations between measured and simulated temperatures can be seen, especially for conditions different from the reference experiment (15 bar, 25 °C, 50/50). For experiments at the conditions of the reference experiments or close to it the deviation in the velocity is very small.

On the other hand, the deviation could originate from the experiments. The mass flow meter and controller (MFC) is in fact supposed to have an accuracy of 2.5 %, as specified by the manufacturer. However, two aspects have to be considered. First, for some experimental conditions the MFC is operated close to the minimum operating flow rate where larger errors are expected. Secondly, the measurement principle of the MFC is based on the heat capacity of the fluid
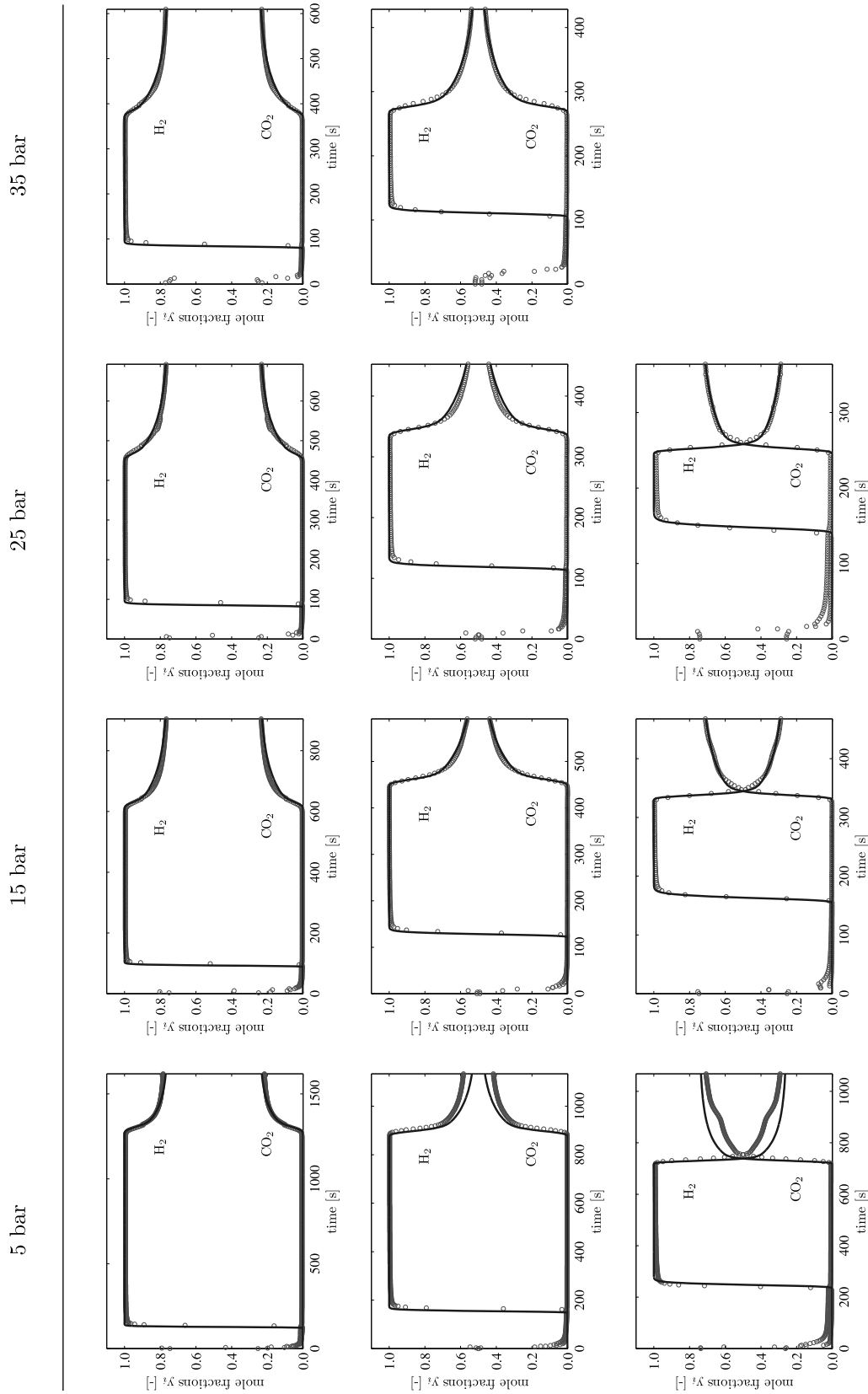
Fig. 6 Exit profiles of experimental (*circle*) and simulated (*line*) breakthrough data at 25 °C for three different CO_2/H_2 mixtures where the CO_2 feed composition increases from the *top* to the *bottom* (25 %, 50 % and 75 %). The transfer parameters are fitted to the experiment carried out at 15 bar, 25 °C feeding a 50/50 CO_2/H_2 mixture, and all the others are predicted
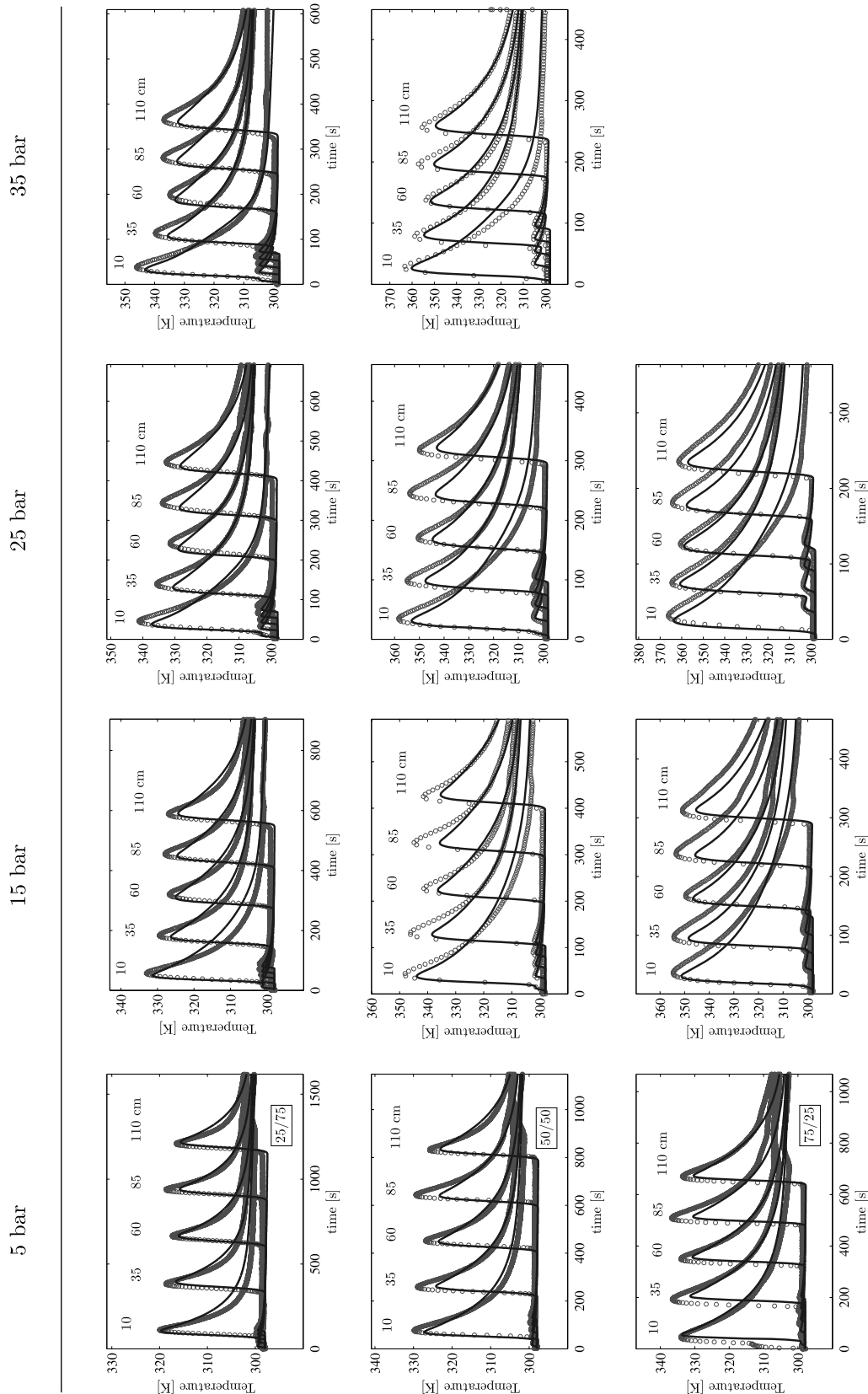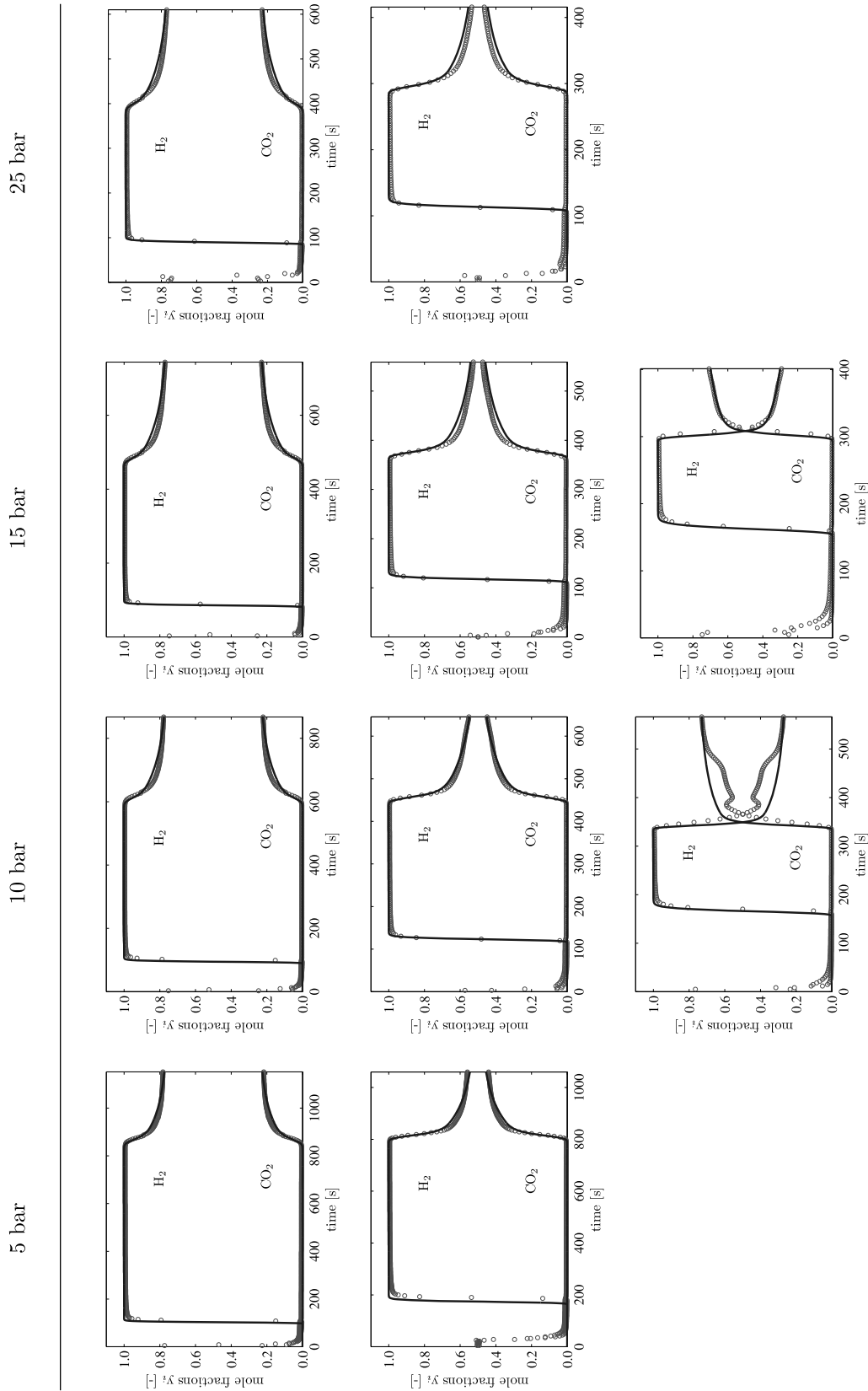
Fig. 7 Temperature profiles of experimental (*circle*) and simulated (*line*) breakthrough data at 25 °C for three different CO_2/H_2 mixtures where the CO_2 feed composition increases from the *top* to the *bottom* (25 %, 50 % and 75 %). The transfer parameters are fitted to the experiment carried out at 15 bar, 25 °C feeding a 50/50 CO_2/H_2 mixture, and all the others are predicted
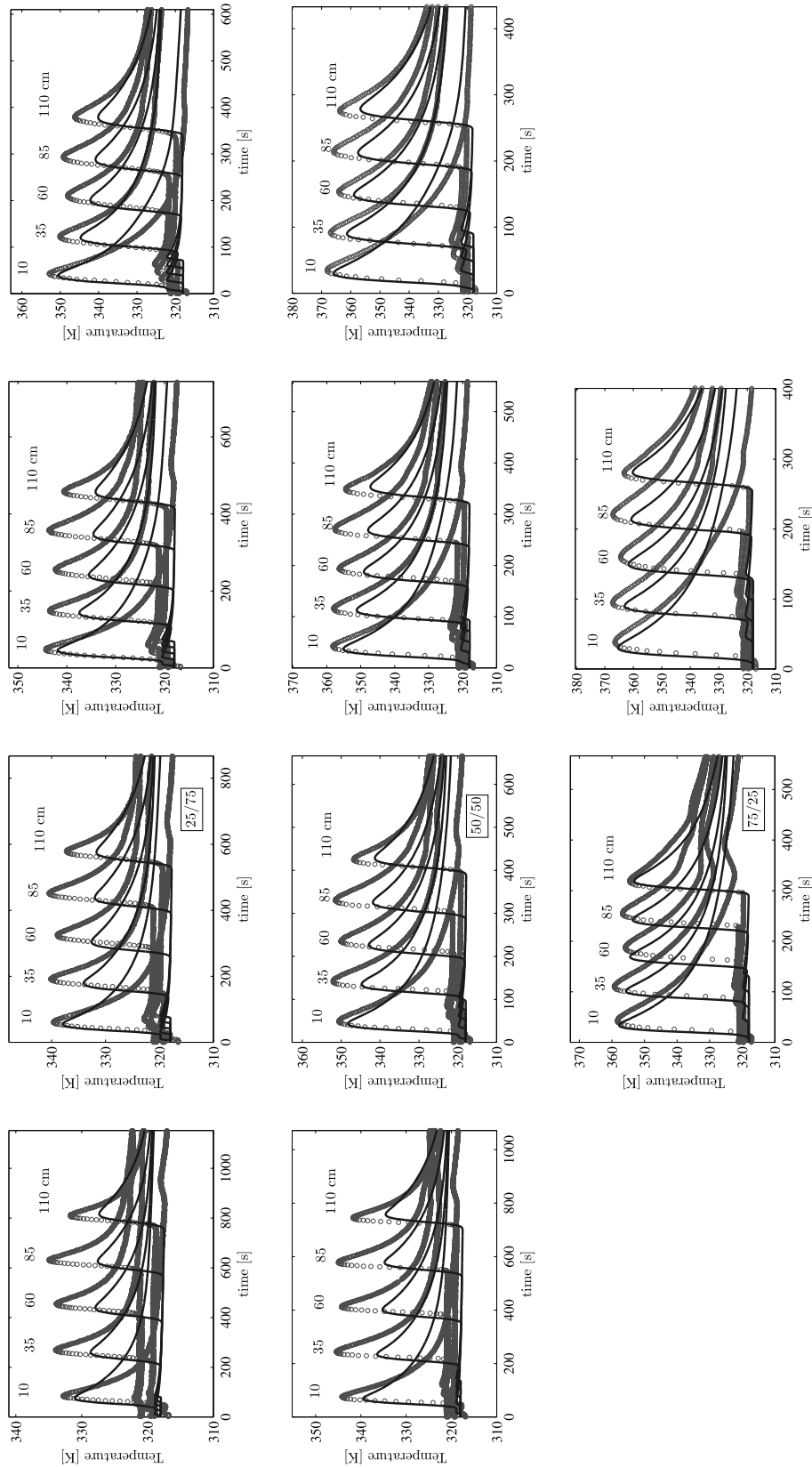
Fig. 8 Exit profiles of experimental (*circle*) and simulated (*line*) breakthrough data at 45 °C for three different CO_2/H_2 mixtures where the CO_2 feed composition increases from the *top* to the *bottom* (25 %, 50 % and 75 %). The transfer parameters are fitted to the experiment carried out at 15 bar, 25 °C feeding a 50/50 CO_2/H_2 mixture, and all the others are predicted

Fig. 9 Temperature profiles of experimental (*circle*) and simulated (*line*) breakthrough data at 45 °C for three different CO_2/H_2 mixtures where the CO_2 feed composition increases from the *top* to the *bottom* (25 %, 50 % and 75 %). The transfer parameters are fitted to the experiment carried out at 15 bar, 25 °C feeding a 50/50 CO_2/H_2 mixture, and all the others are predicted

phase, which is of course a function of temperature, pressure and composition. The MFC is calibrated for a specific gas mixture at specified temperature and pressure conditions. If it is used at different conditions, a calibration factor (provided by the manufacturer) has to be applied and might introduce an error, which—though possibly systematic—is very difficult to correct for.

The trends observed in Fig. 10, which are rather regular though impossible to rationalize beyond what discussed above, seem to indicate that there is some kind of systematic experimental error in the operation and use of the MFC. In the light of this, the velocity values used in the simulation should be interpreted as "fitted" values that, indeed because of the smooth trends observed through a large range of experimental conditions, we view as rather accurate estimates of the real velocities.

4.4 Effect of temperature, pressure and composition

The breakthrough time is conventionally defined in this study as the time, when the mole fraction of the component of choice becomes larger than 0.002. When comparing the

breakthrough times of CO_2 and H_2 at different conditions, as illustrated in Figs. 6 and 8 and summarized in Table 5, the following trends can be observed:
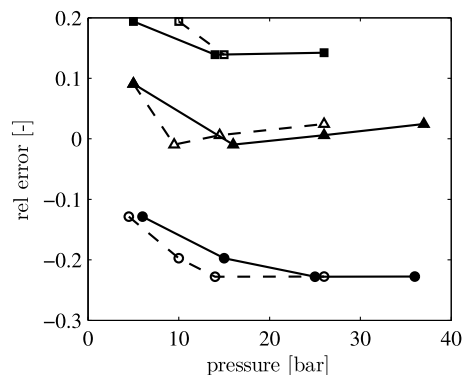

Fig. 10 The relative errors of the feed velocities used in the simulation compared to the actual experimental feed velocities are plotted against pressure. Experiments conducted at $T = 25\,°C$ are represented with filled symbols (e.g ▲) and $T = 45\,°C$ with empty symbols (e.g. △). The three feed mixtures are compared, namely 25/75 CO_2/H_2 (○/●), 50/50 CO_2/H_2 (△ /▲) and 75/25 CO_2/H_2 (□/■)

Table 5 Simulated breakthrough times of H_2 and CO_2 obtained at the different experimental conditions

Feed CO_2/H_2	T [°C]	p [bar]	H_2 [s]	CO_2 [s]
75/25	25	5	175	700
		10	145	420
		15	130	320
		25	120	240
	45	10	125	330
		15	125	285
50/50	25	5	125	875
		10	120	585
		15	105	440
		25	100	325
		35	95	260
	45	5	130	775
		10	95	435
		15	90	355
		25	90	275
25/75	25	5	105	1270
		10	85	795
		15	80	610
		25	75	460
		35	75	370
	45	5	80	835
		10	75	590
		15	70	465
		25	70	380

1. at constant feed composition, the CO_2 breakthrough time decreases with increasing pressure, while the H_2 front is hardly affected;
2. at constant pressure and increasing amount of CO_2 in the feed mixture, the CO_2 breakthrough time decreases, while the H_2 breakthrough time slightly increases;
3. at constant pressure and composition, the CO_2 breakthrough time decreases with increasing process temperature, while the H_2 breakthrough time decreases only slightly.

These observations can be explained by the fact that the breakthrough depends mainly on the adsorption equilibrium at the given conditions and on the amount of moles fed (mol/s). The latter becomes larger at higher pressures, if the volume flow is kept constant. Therefore, the difference between the breakthrough times of CO_2 and H_2 becomes smaller even though more CO_2 is adsorbed at higher pressure.

4.4.1 H_2 production and recovery

Using the validated model, several considerations are worth making with respect to a CO_2/H_2 separation process. The difference between H_2 and CO_2 breakthrough times directly affects the cycle time in a continuous process, such as a PSA process, and therefore the amount of pure H_2 that can be produced per cycle. Accordingly, the same effect of the process conditions on the H_2 production is observed, as on the breakthrough times. As a consequence at higher pressure the amount of pure H_2 that can be produced in one cycle increases, even though the production time decreases, as illustrated exemplary for a 50/50 CO_2/H_2 feed mixture in Fig. 11a. Such a mixture has been selected, because it is very similar in composition to the feed mixture in a typical IGCC power plant. On the contrary, the H_2 recovery, which is defined as the amount of H_2 produced at the specified purity with respect to the amount fed, decreases with increasing pressure, as shown in Fig. 11b, meaning that more H_2 remains in the column by the time CO_2 breaks through. In a continuous process this is accounted for by adjusting the cycle time in such a way that the H_2 loss is minimized. Furthermore, one can observe that at higher temperatures the amount of pure hydrogen that can be produced decreases, due to a shorter production time. The latter depends on the adsorption selectivity at the given conditions and decreases with increasing temperature.

5 Discussion and conclusions

In this work we have reported about breakthrough experiments in a fixed bed adsorber packed with commercial activated carbon involving feed mixtures of carbon dioxide and
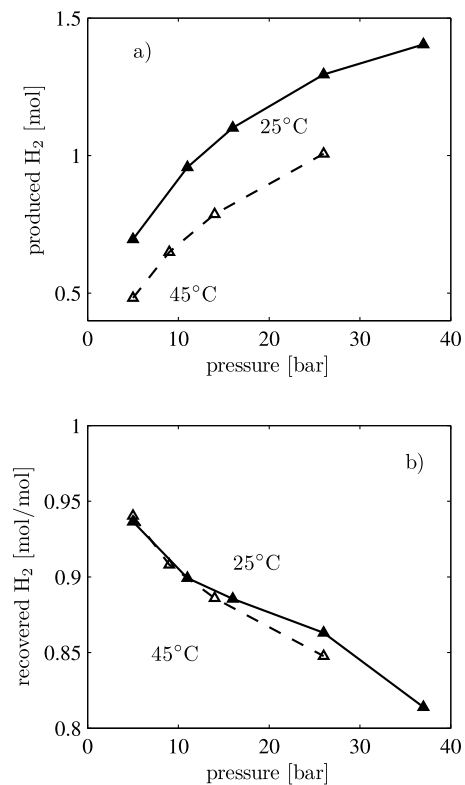

Fig. 11 Comparison of the amount of pure H_2 obtained in a breakthrough experiment for a feed mixture containing 50 % CO_2, given in terms of (**a**) amount produced and (**b**) fraction recovered at two different temperatures, where $T = 25$ °C is represented with filled symbols (▲) and $T = 45$ °C with empty symbols (△)

hydrogen of different compositions. The experiments have been carried out in a broad range of pressures and temperatures, and the experiments at 25 °C and 45 °C have been described using a rather detailed mathematical model. The broad range of operating conditions and the predictive character of the use of the model constitute the novelty of this work.

In the model material and energy balances are coupled through the thermal effects of adsorption, and include constitutive equations of various nature, namely competitive adsorption isotherms that have been characterized as a function of temperature, pressure and composition independently, as reported previously (Schell et al. 2012), as well as the ideal gas law. Only a few transport parameters have been fitted to one reference experiment, whereas the results of all the other experiments have been predicted using the same set of parameters and constitutive equations.

Critical aspects to allow for a meaningful comparison between simulations and experiments have been the modeling of the fluid flow from the packed bed outlet to the detector, namely the mass spectrometer, on the one hand, and of the heat transfer between the column and the heating system on the other. Both phenomena are not easy to describe

in all their details and call necessarily for a certain degree of empiricism and approximation in the modeling as discussed above.

Heat transfer and thermal effects are tightly correlated to the heat absorbed and released upon adsorption and desorption, respectively. Such a heat can be determined based on the adsorption isotherm provided as a function of temperature, thus obtaining the so-called isosteric heat of adsorption as a function of temperature and loading. Although this is in principle possible, in practice the corresponding relationship is very sensitive to the adsorption isotherm selected and to its parameters, as discussed in greater detail in a previous paper (Schell et al. 2012). The temperature dependence of the isosteric heat of adsorption is especially pronounced under certain conditions, whereas the temperature varies significantly during an experiment. As a consequence we have decided to use an average heat of adsorption, i.e. the same at all temperatures and loadings. Although this might look as a drastic simplification, we felt that this represents the most reasonable compromise, and that a more detailed description of the temperature and loading dependence of the heat of adsorption would bring no major improvement in the prediction capabilities of the model, but only additional complexity and computational burden.

The experimental results demonstrate a number of important features of the adsorption behavior of mixtures of carbon dioxide and hydrogen, which have an impact on the possibility of exploiting adsorption in a continuous process (PSA or TSA) for separating the two gases. In particular, it has been possible to assess the role of pressure on the amount of pure hydrogen that can be produced in a single pass.

The mathematical model that we have developed exhibits a level of accuracy that can be judged to be between good and very good depending on the operating conditions. We consider this as a rather good result considering that we have made no adjustment whatsoever on the adsorption isotherms after measuring them in a completely independent manner in a gravimetric set-up (Schell et al. 2012). In order to describe well in the simulations both the position of the temperature peaks (adsorption fronts) along the column, whose measurement is carried out through in-situ thermocouples and is recorded in real time, i.e. without any time delay, and the breakthrough times of the hydrogen and carbon dioxide fronts at the column outlet, which are measured at the MS detector, i.e. with time delay, we have been forced to make an adjustment of the gas velocity in the simulations with respect to the set-point value in the experiments. As discussed above, this might be due to either the intrinsic inaccuracy of the mass-flow meter and controller, particularly at small values of the flow rate, or the systematic error in the determination of the calibration factor as a function of temperature, pressure and composition, or the mismatch between,

for instance, the simplified description of heat transfer in the model and the reality of the complex structure of the heating jacket installed on the experimental fixed bed adsorber.

In spite of these difficulties, we are convinced that the model that we have developed captures all the crucial phenomena and predicts all the important trends observed in the separation of carbon dioxide and hydrogen by adsorption on activated carbons, and that it does so in a quantitative manner. This will allow us to use the model for process design and optimization.

We also believe that this study, thanks to its painstaking character and comprehensive scope, provides valuable insight into the issues encountered and trade-offs needed in studying such a complex system as non-isothermal competitive gas adsorption in a fixed bed. Complexity stems from the strong coupling among the different phenomena, which makes parameter estimation difficult and limits somehow the predictive capability of the model. Moreover, experimental set-ups dealing with high-pressure gases and non-isobaric conditions are intrinsically more difficult to operate and to control than for instance preparative liquid chromatography systems. We strongly believe that the wealth of data reported in this work, particularly in Figs. 6 to 9, and the methods and tools used to analyze them can be very valuable for researchers and practitioners interested in adsorption based systems to be applied in carbon dioxide capture systems.

References

Arstad, B., Fjellvåg, H., Kongshaug, K., Swang, O., Blom, R.: Amine functionalised metal organic frameworks (MOFs) as adsorbents for carbon dioxide. Adsorption **14**(6), 755–762 (2008)

Belmabkhout, Y., Sayari, A.: Isothermal versus non-isothermal adsorption desorption cycling of triamine-grafted pore-expanded MCM-41 mesoporous silica for CO2 capture from flue gas. Energy Fuels **24**(9), 5273–5280 (2010)

Do, D.: Adsorption Analysis: Equilibria and Kinetics. Imperial College Press, London (1998), pp. 57–64, chapter 3.2.2

Haynes, W.M.: CRC Handbook of Chemistry and Physics, 92th edn. CRC Press, Boca Raton (2011)

Herm, Z.R., Swisher, J.A., Smit, B., Krishna, R., Long, J.R.: Metal-organic frameworks as adsorbents for hydrogen purification and precombustion carbon dioxide capture. J. Am. Chem. Soc. **133**(15), 5664–5667 (2011)

IPCC: IPCC Special Report on Carbon Capture and Storage. Cambridge University Press, Cambridge (2005)

IPCC: Climate Change 2007: Synthesis Report. Cambridge University Press, Cambridge (2007)

Javeed, S., Qamar, S., Seidel-Morgenstern, A., Warnecke, G.: Efficient and accurate numerical simulation of nonlinear chromatographic processes. Comput. Chem. Eng. **35**(11), 2294–2305 (2011)

Kim, J.-N., Chue, K.-T., Kim, K.-I., Cho, S.-H., Kim, J.-D.: Non-isothermal adsorption of nitrogen-carbon dioxide mixture in a fixed bed of zeolite-X. J. Chem. Eng. Jpn. **27**(1), 45–51 (1994)

Leva, M.: Heat transfer to gases through packed tubes. Ind. Eng. Chem. **39**(7), 857–862 (1947)

LeVeque, R.J.: Finite Volume Methods for Hyperbolic Problems. Cambridge University Press, Cambridge (2002)

Lin, W., Farooq, S.: Estimation of overall effective coefficient of heat transfer for nonisothermal fixed-bed adsorption. Chem. Eng. Sci. **54**, 4031–4040 (1999)

Lopes, F.V.S., Grande, C.A., Rodrigues, A.E.: Activated carbon for hydrogen purification by pressure swing adsorption. Multicomponent breakthrough curves and PSA performance. Chem. Eng. Sci. **66**(3), 303–317 (2011)

Malek, A., Farooq, S.: Hydrogen purification from refinery fuel gas by pressure swing adsorption. AIChE J. **44**(9), 1985–1992 (1998)

Mulgundmath, V.P., Jones, R.A., Tezel, F.H., Thibault, J.: Fixed bed adsorption for the removal of carbon dioxide from nitrogen: breakthrough behaviour and modelling for heat and mass transfer. Sep. Purif. Technol. **85**, 12–27 (2012)

NIST: NIST Chemistry WebBook (2011). http://webbook.nist.gov/chemistry

Park, J.-H., Kim, J.-N., Cho, S.-H.: Performance analysis of four-bed H2 PSA process using layered beds. AIChE J. **46**(4), 790–802 (2000)

Kim, J.-N., Kim, K.-I., Cho, S.-H., Kim, J.-D., Yang, R.T.: Adsorber dynamics and optimal design of layered beds for multicomponent gas adsorption. Chem. Eng. Sci. **53**(23), 3951–3963 (1998)

Perry, R.H., Green, D.W., Maloney, J.O.: Perry's Chemical Engineers' Handbook. McGraw-Hill, New York (1984)

Rohsenow, W.M., Hartnett, J.P., Ganić, E.N.: Handbook of Heat Transfer Applications, 2nd edn. McGraw-Hill, New York (1985)

Ruthven, D.: Principles of Adsorption and Adsorption Processes. Wiley, New York (1984)

Ruthven, D., Farooq, S., Knaebel, K.: Pressure Swing Adsorption. VCH, Weinheim (1994)

Schell, J., Casas, N., Pini, R., Mazzotti, M.: Pure and binary adsorption of CO2, H2 and N2 on activated carbon. Adsorption **18**(1), 49–65 (2012)

Taczyk, M., Warmuziski, K.: Multicomponent pressure swing adsorption. Part II. Experimental verification of the model. Chem. Eng. Process. **37**(4), 301–315 (1998)

U.S. Department of Energy: DOE/NETL Carbon Dioxide Capture and Storage RD&D Roadmap (2010)

U.S. Energy Information Administration: International Energy Outlook 2011 (2011)

Webley, P.A., He, J.: Fast solution-adaptive finite volume method for PSA/VSA cycle simulation; 1 single step simulation. Comput. Chem. Eng. **23**(11–12), 1701–1712 (2000)

Zhou, L., Li, J., Su, W., Sun, Y.: Experimental studies of a new compact design four-bed PSA equipment for producing oxygen. AIChE J. **51**(10), 2695–2701 (2005)